Scientific Research Publishing

International Journal of Geosciences, 2024, 15, 1020-1037
https://www.scirp.org/journal/ijg
ISSN Online: 2156-8367
ISSN Print: 2156-8359

Petrography and Mineral Chemistry of Metamorphogenic Magnetite in the Layered Sill of the JC Pura Schist Belt, Karnataka, India

B. G. Dayanand, S. Santhosh, B. C. Prabhakar

Department of Geology, Bangalore University, Bangalore, India
Email: dayanandbg@bub.ernet.in, santhosh@bub.ernet.in, bcprabhakar@rediffmail.com

How to cite this paper: Dayanand, B.G., Santhosh, S. and Prabhakar, B.C. (2024) Petrography and Mineral Chemistry of Metamorphogenic Magnetite in the Layered Sill of the JC Pura Schist Belt, Karnataka, India. *International Journal of Geosciences*, **15**, 1020-1037.
https://doi.org/10.4236/ijg.2024.1512054

Received: November 13, 2024
Accepted: December 20, 2024
Published: December 23, 2024

Abstract

JC Pura schist belt has gained scope recently with reports of nickel, magnetite, PGEs, and traces of gold. The layered sill in the schist belt is a linear patch of ultramafic sequences (peridotite and pyroxenite) with metamorphogenic magnetite mineralization. The metamorphogenic magnetite appears as interbands in layered sequences and as veins in serpentinite. The present study focuses on understanding the characteristics of metamorphogenic magnetite by petrographic and EPMA analysis. The study found that the precursor chromite grains are transformed into Cr-magnetite and magnetite in the spinel transformation system due to metamorphism and hydrothermal alteration. The Cr, Mg, Al, and Ni are depleted during transformation, and Fe is enriched. The Cr-magnetite appears homogenous in the vein due to serpentinization, indicating prograde greenschist to amphibolite facies metamorphism, and the area has suffered an episodic metamorphic process. The results of Cr-magnetite cation proportions of Cr fall within ishkulite variety data range of 0.10 - 0.50 apfu (atoms per formula unit). Cr-magnetite variety Ishkulite represents an additional miscibility gap in the Cr-Fe^{3+} transformation series other than ferrite chromite and chrome magnetite. The transformation process primarily involves the oxidation of chromium and the reduction of iron. The oxidation of chromite by highly oxidizing fluids with increasing pressure and temperature alters to Cr-magnetite, where chromium in the +3 state oxidizes to the +6 state, forming soluble chromate ions and diffusing with Fe^{3+}. Then, it transforms into magnetite due to reducing conditions. Cr-magnetite vein indicates the potential for chromite deposits in the area, and hydrothermal altered magnetites could be a source for hosting valuable precious metals like gold and PGEs. Further investigations are needed to assess the mineralization potential and its extent.

Keywords

JC Pura, Layered Sill, Metamorphogenic Magnetite, Cr-Magnetite, Ishkulite

1. Introduction

Layered intrusion outcrop areas are limited compared to many mafic intrusive bodies globally. Their origin is reported throughout geological time, from Archaean to Cenozoic, and they vary in size from less than a square kilometer to tens of thousands of square kilometers. Many layered intrusions occur within Archaean craton [1], and global examples include the Bushweld Complex (South Africa), Great Dyke (Zimbabwe), Stillwater Complex (Montana), Norlilsk Talnakh (Russia), Pilbara (Australia), and Labrador Tough (Canada). These layered intrusions represent ultramafic to mafic litho-sequences with textural and compositional variations and are commonly associated with extrusive komatiite [2]-[8]. The layering is formed due to fractional crystallization by the differential settling process. The layered Intrusions are of significant economic importance as they are known to host base metals and associated precious metals.

Very few layered intrusions have been reported in Indian cratonic blocks. In the Dharwar craton, the layered sequence rocks are seen in the Nuggihalli schist belt and the Hanumalapura complex of West Dharwar Craton; the Kondapalli layered complex and the Sittampudi anorthosite complex of East Dharwar Craton. JC Pura schist belt lacks economic significance compared with other Dharwar schist belts even though they all evolved during Archean. In most of the earlier works, the petrological, textural, and structural characterization has been carried out in the JC Pura schist belt [6] [9]. Also, the layered sill of the ultramafic sequence has been reported from the JC Pura schist belt [10] [11]. In the recent findings, the scope for the JC Pura schist belt has opened up with the preliminary reporting of PGEs and trace elements like Cr, Ni, Fe, and Ti [12] [13] and traces of gold in magnetite grains [14]. The present study focuses on the layered ultramafic sill of the JC Pura schist belt. During our fieldwork, magnetite mineralization was observed as layered bands within the layered sill body and vein-type in adjacent serpentinized komatiites. Petrography and ore mineral phases were characterized for the samples collected during fieldwork to identify the mineralization type and understand compositional variations.

2. Geology

JC Pura schist belt is an oval-shaped Archaean greenstone belt in the western Dharwar craton (**Figure 1**), dating back to 3.23 - 3.35 Ga [5] [15]. The rocks of the JC Pura schist belt are considered to be Sargur equivalent [16], and the Dharwar group overlies these Sargur group rocks with an angular unconformity along the Kibbanahalli arm of the Chitradurga schist belt [15]. The JC Pura schist

belt appears as a dome in its central portion due to the granitoid intrusion [9] [17]. The predominant rock types of the JC Pura belt are extrusive ultramafic rocks (dunite, peridotite, pyroxenite), basalts (amphibolite), minor cherty meta quartzites, and rare banded iron formation (BIF). The ultramafic rocks exhibit komatiitic characteristics and are intensely serpentinized, chloritized, and carbonatized. The talc-chlorite-tremolite schist indicates greenschist to lower amphibolite

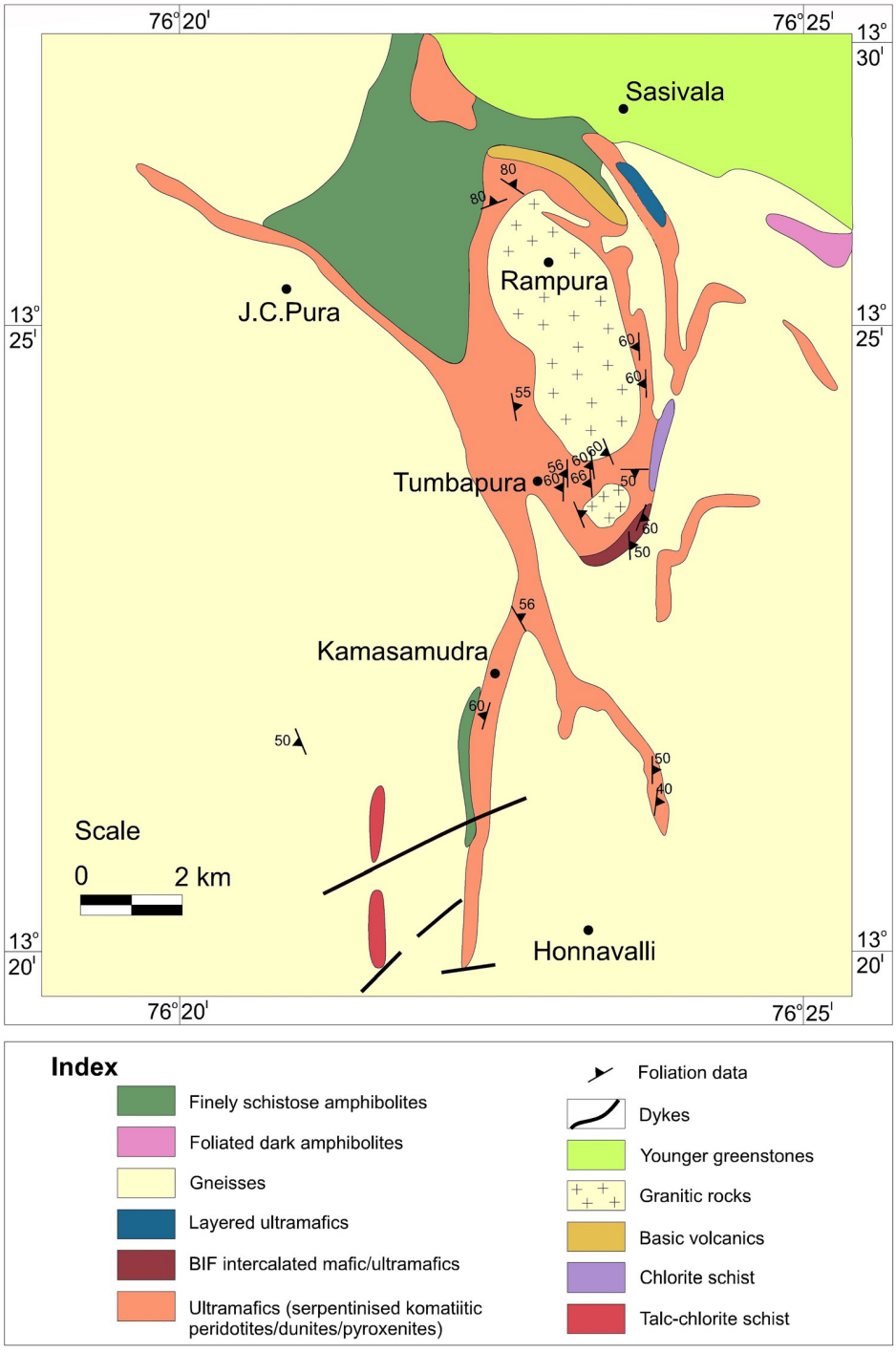

Figure 1. Geology map of JC Pura Schist Belt (after Venkatadasu *et al.*, 1991).

facies metamorphism [6]. These Sargur equivalent rocks are surrounded by Peninsula Gneiss emplaced as synkinematic intrusions followed by granitic activity. The intrusive layered sill body is found within the extrusive komatiitic milieu of the JC Pura schist belt [10]. The layered sill is about 1 kilometer in length and 200 meters in width. Its lithology includes dunite, peridotite, and pyroxenite. All these rocks are partially to completely altered to serpentinite. The ultramafic sequences are of cyclic type with sharp contacts, which could be the result of episodic injection of undifferentiated to slightly differentiated magma pulses which solidified without much fractional crystallization [10] [18] [19]. Magnetite is noticed as band within a layered sill (**Figure 2(a)** & **Figure 2(b)**), and sometimes it cuts across serpentinite (**Figure 3(a)** & **Figure 3(b)**) showing feeble to moderate magnetism. Magnetite crystals are also seen as rolled grains near the layered sill and are oxidized. Magnetite vein width ranges from 2 - 4 cm. The serpentinite outcrops exhibit skeletal features due to weathering.

(a) (b)

Figure 2. (a) Layering of serpentinized peridotite and pyroxenite with interbands of chromium bearing magnetite. (b) Cumulus zoning of relict ferro silicates noticed on the surface of serpentinized pyroxenites.

(a) (b)

Figure 3. (a) Centimetric scale Cr-magnetite vein in serpentinite. (b) Cr-magnetite as coarse stringer and inclusions in serpentinite.

3. Methods

During fieldwork, the rock samples bearing mineralization were collected from the layered sill randomly. Five samples were chosen, and doubly polished thin section slides were prepared for petrographic and electron probe microanalyzer (EPMA) studies to understand the mineral phases and their characteristics. The mineral phases present in the studied rock were analyzed by deploying CAMECA-SX Five Electron Probe Micro Analyzer (EPMA) at the Department of Geology, Centre of Advanced Study, Institute of Science, Banaras Hindu University. Before analysis, the thin section was coated with a 20 nm carbon layer LEICA-EM ACE200 instrument for better conductivity. The CAMECA SXFive instrument was operated using a LaB6 filament source, at 15 kV accelerating voltage and 10 nA current. Wavelength dispersive X-ray spectrometry in combination with LIF (lithium fluoride), PET (penta erythritol), LPET (long penta erythritol), TAP (thallium acid phthalate), LTAP (long thallium acid phthalate) and PC1 crystals were deployed for the quantitative analyses. The beam's diameter and peak time throughout the analysis was ~1 μm and 10 ns, respectively. X-ray intensities were calculated by using the X-PHI correction. The instrument was calibrated using the CAMECA natural and synthetic standards. The detailed procedure is documented in Pandey *et al.* [20].

4. Results

4.1. Petrography

The petrographic study reveals that the layered ultramafic sequences are intensely serpentinized and transformed into serpentinite. Remnants of olivine and pyroxenes are preserved as fragmented grains (**Figure 4(a)**). Chloritic and carbonate alterations are also observed. The cumulus grains of altered pyroxenes, amphiboles (tremolite), and subhedral carbonate grains with scattered opaques could be seen (**Figure 4(b)**). The development of talc, carbonates, and chlorite grains in interlocking serpentinites suggests that carbonatization and chlorination are the latter of serpentinization processes. Tiny pyroxene cumulates exhibit complex textures similar to the serpentinite aggregate-like mass (**Figure 5(a)**). The fine-grained opaques are scattered throughout as dissemination and appear as dense clouding at places within silicates (**Figure 5(b)**).

Under a reflected light microscope, the magnetite appears as scattered tiny fragments, coarse-grained, euhedral to subhedral shaped grains in layered bands; and cumulative massive grains in veins (**Figure 6(a)**). Minor amounts of subhedral to anhedral chromite grains are seen with magnetite as interstitial grains with silicate minerals. The ilmenite is seen as exsolved lamellae on the magnetite grains (**Figure 6(b)**).

4.2. Mineral Chemistry

The Back Scattered Electron (BSE) images of selected mineral phases (**Figures 7(a)-(d)**) and the EPMA results data of major and minor elements (**Table 1**) are presented below.

The oxide ore mineral phases are Cr-magnetite (Table 2) and magnetite (Table 3). The end members of the oxy spinel subgroup are considered for calculation from the spinel supergroup based on IMA-CNMNC (Commission on New Minerals, Nomenclature, and Classification of the International Mineralogical Association) [21] [22]. The Cr-magnetite has FeO content ranging between 73.98 and

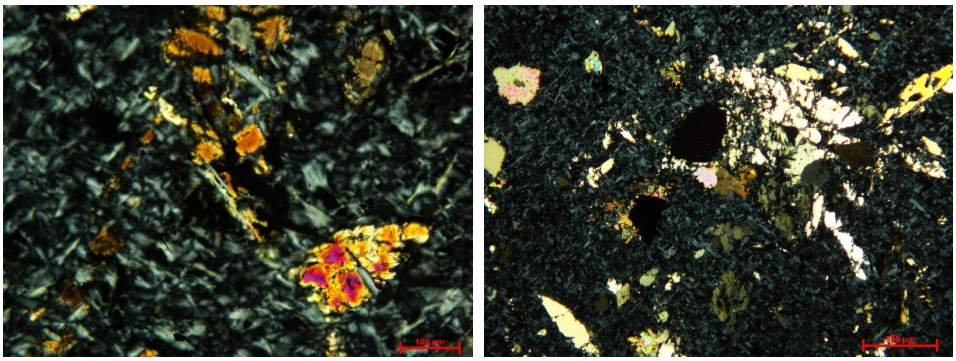

(a) (b)

Figure 4. (a) Serpentinite with relicts of olivine (yellow tints) and pyroxene (green to brown and elongated grains). (b) Cumulus grains of altered pyroxenes, tremolite, talc, subhedral carbonate and chlorite grains in serpentinite.

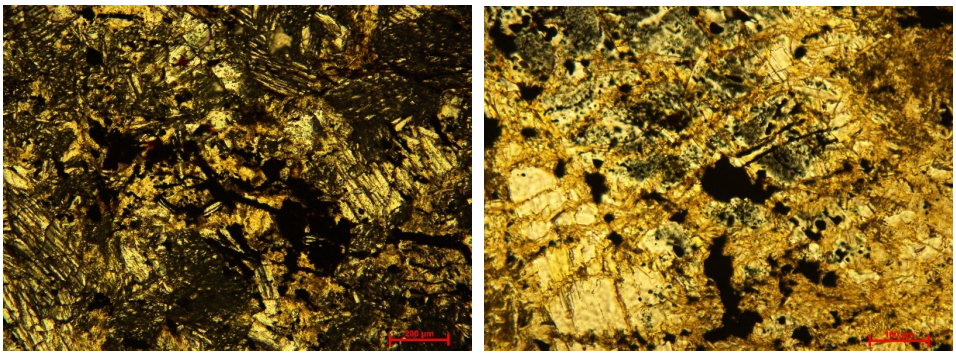

(a) (b)

Figure 5. (a) Cumulus altered pyroxene crystal exhibiting complex texture. (b) Opaques appearing as dense clouding.

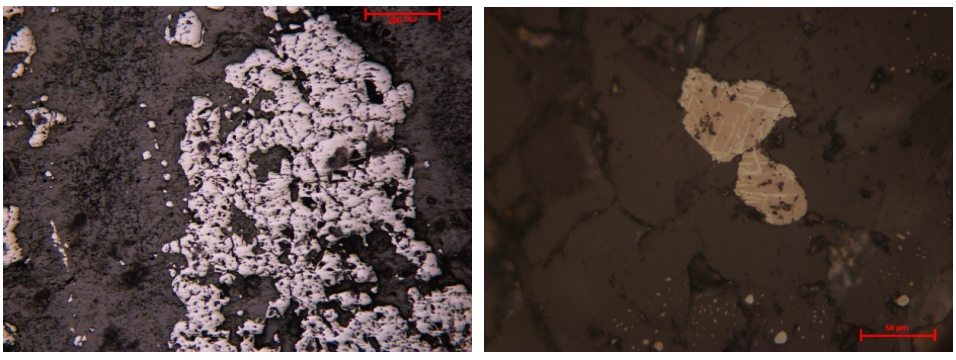

(a) (b)

Figure 6. (a) Massive magnetite grains with minor amount of accessory chromite. (b) Ilmenite as exsolved lamellae in magnetite grains.

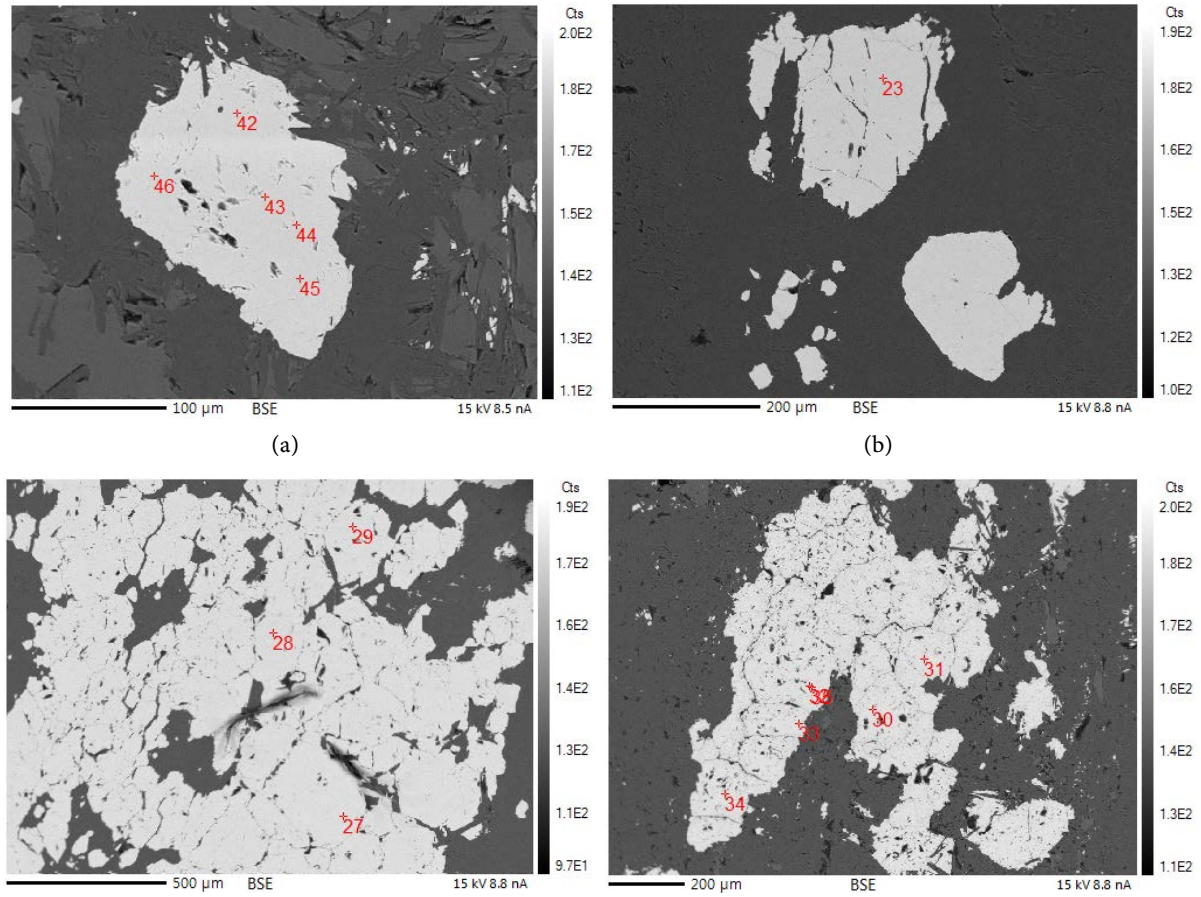

Figure 7. Backscattered Electron (BSE) images of metamorphogenic magnetite grains of JC Pura layered sill: (a) (b) Cr-magnetite and magnetite grains in layered bands; (c) (d) Massive homogenous Cr-magnetite grains in vein.

91.18 wt%; Cr_2O_3: 2.67 - 14.79 wt%; MgO: 0.0038 - 16.05 wt%; Al_2O_3: 0 - 1.98 wt%; MnO: 0.0049 - 1.85 wt%; TiO_2: 0 - 1.02; and NiO: 0.1 - 0.68 wt%, respectively. The cation proportions of Cr-magnetite show the average contents of Cr - 0.2037 apfu (Atoms per formula unit); Fe^{3+} - 1.7052 apfu; Fe^{2+} - 0.9578; Mg - 0.043 apfu; Al - 0.011 apfu; Mn - 0.015 apfu; Ni - 0.016 apfu; and Ti - 0.0073 apfu. The cation proportion ratio of Cr# [Cr/(Cr+Al)] range from 0.97 - 1 atomic ratios; Mg# [Mg/(Fe^{2+}+ Mg)] range from 0.0013 - 0.0470 atomic ratios; and Fe^{3+}/R^{3+} (R^{3+} = Fe^{3+}+ Cr + Al) range from 0.77 - 0.96 atomic ratios. The magnetite FeO composition ranges from 70.67 - 78.11 wt%. The cation proportions of magnetite show the high contents of Fe^{3+} - 1.7211 apfu, and Fe^{2+} - 1.1122 apfu. Other elements like V, Ti, Cr, Ni, Mg, and Al are present in very minor proportions. The cation proportions ratio of Fe^{3+}/R^{3+} ranges from 0.99 - 1 atomic ratios and Fe^{2+}#[Fe^{2+}/(Fe^{2+}+Mg)] range from 0.97 - 1 atomic ratios.

Table 1. EPMA compositional data of major and minor element oxides in weight percentage for selected grains.

Sample No.	Point No.	SiO_2	TiO_2	Al_2O_3	Cr_2O_3	FeOT	MnO	MgO	CaO	Na_2O	K_2O	NiO	Total	Fe_2O_3	FeO	Total
JCB1	42/1	0.01	0.09	0.04	5.18	88.71	0.36	0.04	0.10	0.01	0.04	0.37	94.93	64.51	30.66	101.39

Continued

JCB1	43/1	0.04	0.16	0.04	6.11	86.46	0.37	0.05	0.06	0.00	0.03	0.67	93.92	62.72	30.01	100.20
JCB1	44/1	0.03	0.27	0.08	5.55	86.75	0.35	0.03	0.05	0.00	0.02	0.56	93.62	62.76	30.28	99.91
JCB1	45/1	0.01	0.23	0.00	3.77	88.23	0.33	0.03	0.04	0.01	0.02	0.39	93.04	64.43	30.25	99.50
JCB1	46/1	0.02	0.10	0.00	4.69	90.00	0.32	0.06	0.08	0.02	0.06	0.46	95.77	65.90	30.70	102.36
JCB3	23/1	0.00	0.97	0.05	14.06	75.84	1.85	0.55	0.04	0.03	0.01	0.42	93.82	52.56	28.55	99.08
JCB3	27/1	0.00	0.99	0.08	14.42	75.23	1.84	0.78	0.05	0.03	0.00	0.31	93.72	52.13	28.32	98.94
JCB3	28/1	0.00	1.02	0.03	14.61	73.98	1.85	0.77	0.04	0.02	0.00	0.39	92.71	51.14	27.96	97.83
JCB3	29/1	0.00	0.92	0.07	14.79	74.54	1.77	0.66	0.03	0.03	0.00	0.58	93.40	51.55	28.15	98.57
JCB4	30/1	0.39	0.10	0.14	6.47	82.73	0.36	0.07	0.12	0.00	0.00	0.37	90.75	58.89	29.74	96.64
JCB4	31/1	0.00	0.11	0.02	6.23	82.95	0.08	0.02	0.05	0.00	0.00	0.00	89.48	59.28	29.61	95.42
JCB4	32/1	0.08	0.10	0.00	5.93	83.37	0.11	0.05	0.03	0.00	0.02	0.21	89.90	59.81	29.55	95.89
JCB4	33/1	0.80	0.19	0.12	6.40	76.34	0.09	0.08	0.09	0.26	0.80	0.26	85.43	56.41	25.58	91.08
JCB4	34/1	0.02	0.12	0.00	6.37	83.60	0.13	0.02	0.03	0.00	0.01	0.00	90.32	59.71	29.87	96.30
JCBG	35/1	0.02	0.13	0.00	2.80	88.92	0.29	0.08	0.05	0.02	0.00	0.42	92.71	65.43	30.04	99.27
JCBG	39/1	0.00	0.19	0.00	3.25	89.72	0.16	0.06	0.01	0.02	0.03	0.56	94.01	65.86	30.46	100.60
JCBG	40/1	0.01	0.08	0.00	3.08	90.90	0.13	0.03	0.03	0.02	0.00	0.68	94.97	66.91	30.69	101.67
JCBG	41/1	0.00	0.10	0.00	2.68	91.18	0.02	0.02	0.04	0.02	0.00	0.34	94.39	66.88	31.00	101.09
JCBG	42/1	0.01	0.20	0.00	3.02	90.19	0.11	0.05	0.08	0.05	0.03	0.43	94.17	66.31	30.52	100.81
JCBG	43/1	0.00	0.04	0.00	3.31	88.99	0.26	0.07	0.02	0.16	0.02	0.41	0.00	66.04	29.56	99.89
JCB4	36/1	6.73	0.00	1.14	0.26	64.06	0.13	0.34	0.50	0.52	0.34	0.89	74.90	39.72	28.32	78.88
JCB4	37/1	5.83	0.00	0.94	0.06	60.80	0.01	0.42	3.93	0.31	0.18	1.42	73.90	41.33	23.61	78.04
JCB5	46/1	0.44	0.03	0.44	0.02	76.07	0.07	0.03	0.02	0.00	0.01	0.28	77.39	55.63	26.01	82.96
JCB5	47/1	2.69	0.00	0.01	0.00	72.16	0.04	0.06	0.18	0.34	0.07	0.49	76.04	50.98	26.28	81.14
JCB5	48/1	2.84	0.02	0.00	0.00	76.91	0.04	0.01	0.11	0.08	0.03	0.05	80.08	52.52	29.65	85.34
JCB5	49/1	3.49	0.02	0.00	0.00	74.22	0.00	0.09	0.18	0.37	0.05	0.07	78.50	50.84	28.47	83.59
JCB5	50/1	3.55	0.00	0.00	0.03	74.55	0.00	0.08	0.26	0.41	0.03	0.11	79.03	51.21	28.46	84.16
JCB5	51/1	3.09	0.01	0.01	0.00	76.43	0.09	0.04	0.14	0.00	0.00	0.08	79.89	51.43	30.15	85.04
JCB5	52/1	3.39	0.02	0.00	0.00	74.82	0.11	0.00	0.15	0.00	0.00	0.23	78.72	49.79	30.02	83.70
JCB5	53/1	3.13	0.00	0.00	0.02	76.68	0.05	0.00	0.10	0.00	0.00	0.10	80.09	51.49	30.35	85.24
JCB5	54/1	3.11	0.00	0.02	0.00	75.76	0.04	0.01	0.19	0.05	0.00	0.00	79.17	51.06	29.81	84.29
JCB5	55/1	2.64	0.04	0.00	0.00	75.49	0.08	0.05	0.17	0.02	0.05	0.22	78.75	51.85	28.84	83.94
JCB5	56/1	3.04	0.00	0.00	0.04	75.88	0.04	0.06	0.13	0.02	0.01	0.22	79.45	51.33	29.69	84.59
JCB5	57/1	3.36	0.00	0.00	0.00	77.12	0.03	0.01	0.08	0.04	0.00	0.09	80.74	51.54	30.74	85.90
JCB5	58/1	3.13	0.01	0.00	0.00	75.94	0.09	0.01	0.06	0.00	0.00	0.20	79.43	50.97	30.07	84.54
JCB5	59/1	3.02	0.00	0.02	0.00	75.25	0.03	0.01	0.11	0.00	0.00	0.18	78.62	50.67	29.66	83.70
JCB5	60/1	2.68	0.00	0.00	0.00	74.63	0.09	0.02	0.20	0.07	0.00	0.11	77.80	51.20	28.56	82.93
JCB5	61/1	2.92	0.02	0.00	0.04	75.28	0.01	0.04	0.13	0.00	0.00	0.34	78.76	50.98	29.40	83.87

Continued

JCB5	64/1	3.69	0.00	0.01	0.01	75.34	0.08	0.02	0.05	0.00	0.00	0.38	79.58	49.67	30.64	84.56
JCB5	65/1	3.89	0.00	0.00	0.00	75.45	0.11	0.01	0.10	0.00	0.01	0.09	79.65	49.27	31.11	84.58
JCB5	66/1	3.81	0.01	0.00	0.01	77.48	0.00	0.01	0.11	0.00	0.02	0.32	81.78	51.04	31.55	86.89
JCB5	67/1	3.82	0.00	0.01	0.00	74.35	0.17	0.02	0.07	0.00	0.00	0.23	78.66	48.71	30.52	83.54
JCB5	68/1	3.31	0.01	0.00	0.00	78.12	0.01	0.16	0.08	0.00	0.00	0.42	82.11	52.58	30.80	87.37
JCB5	69/1	3.93	0.01	0.00	0.00	74.89	0.00	0.00	0.05	0.00	0.00	0.21	79.09	48.69	31.07	83.97
JCB5	70/1	3.70	0.01	0.00	0.00	74.40	0.06	0.06	0.10	0.02	0.02	0.15	78.52	49.01	30.30	83.43

Table 2. Cation proportions (apfu) of Cr-magnetites.

Cation (apfu)	**Cr-Magnetite**																			
Sample No.	**JCB1**	**JCB1**	**JCB1**	**JCB1**	**JCB1**	**JCB3**	**JCB3**	**JCB3**	**JCB3**	**JCB4**	**JCB4**	**JCB4**	**JCB4**	**JCB4**	**JCBG**	**JCBG**	**JCBG**	**JCBG**	**JCBG**	**JCBG**
Si	0.00	0.00	0.00	0.00	0.00	0.00	0.00	0.00	0.00	0.02	0.00	0.00	0.03	0.00	0.00	0.00	0.00	0.00	0.00	0.00
Ti	0.00	0.00	0.01	0.01	0.00	0.03	0.03	0.03	0.03	0.00	0.00	0.00	0.01	0.00	0.00	0.01	0.00	0.00	0.01	0.00
Al	0.00	0.00	0.00	0.00	0.00	0.00	0.00	0.00	0.00	0.01	0.00	0.00	0.01	0.00	0.00	0.00	0.00	0.00	0.00	0.00
Cr	0.16	0.19	0.17	0.12	0.14	0.43	0.44	0.45	0.45	0.20	0.20	0.19	0.21	0.20	0.09	0.10	0.09	0.08	0.09	0.10
Fe^{3+}	1.84	1.81	1.81	1.87	1.86	1.52	1.50	1.49	1.49	1.75	1.79	1.80	1.77	1.79	1.91	1.89	1.90	1.91	1.90	1.91
Fe^{2+}	0.97	0.96	0.97	0.98	0.96	0.92	0.91	0.91	0.91	0.98	1.00	0.99	0.89	1.00	0.97	0.97	0.97	0.99	0.97	0.95
Mn	0.01	0.01	0.01	0.01	0.01	0.06	0.06	0.06	0.06	0.01	0.00	0.00	0.00	0.00	0.01	0.01	0.00	0.00	0.00	0.01
Mg	0.00	0.00	0.00	0.00	0.00	0.03	0.04	0.04	0.04	0.00	0.00	0.00	0.00	0.00	0.00	0.00	0.00	0.00	0.00	0.00
Ca	0.00	0.00	0.00	0.00	0.00	0.00	0.00	0.00	0.00	0.01	0.00	0.00	0.00	0.00	0.00	0.00	0.00	0.00	0.00	0.00
Na	0.00	0.00	0.00	0.00	0.00	0.00	0.00	0.00	0.00	0.00	0.00	0.00	0.02	0.00	0.00	0.00	0.00	0.00	0.00	0.01
K	0.00	0.00	0.00	0.00	0.00	0.00	0.00	0.00	0.00	0.00	0.00	0.00	0.04	0.00	0.00	0.00	0.00	0.00	0.00	0.00
Ni	0.01	0.02	0.02	0.01	0.01	0.01	0.01	0.01	0.02	0.01	0.00	0.01	0.01	0.00	0.01	0.02	0.02	0.01	0.01	0.01
Total	**3.00**	**3.00**	**3.00**	**3.00**	**3.00**	**3.00**	**3.00**	**3.00**	**3.00**	**3.00**	**3.00**	**3.00**	**3.00**	**3.00**	**3.00**	**3.00**	**3.00**	**3.00**	**3.00**	**3.00**
Cr#	0.99	0.99	0.98	1.00	1.00	0.99	0.99	1.00	0.99	0.97	0.99	1.00	0.97	1.00	1.00	1.00	1.00	1.00	1.00	1.00
Mg#	0.00	0.00	0.00	0.00	0.00	0.03	0.05	0.05	0.04	0.00	0.00	0.00	0.01	0.00	0.01	0.00	0.00	0.00	0.00	0.00
Fe#	1.00	1.00	1.00	1.00	1.00	0.97	0.95	0.95	0.96	1.00	1.00	1.00	0.99	1.00	0.99	1.00	1.00	1.00	1.00	1.00
Fe^{3+}/R^{3+}	0.92	0.91	0.91	0.94	0.93	0.78	0.77	0.77	0.77	0.89	0.90	0.91	0.89	0.90	0.96	0.95	0.95	0.96	0.95	0.95
End Members																				
Sample No.	**JCB1**	**JCB1**	**JCB1**	**JCB1**	**JCB1**	**JCB3**	**JCB3**	**JCB3**	**JCB3**	**JCB4**	**JCB4**	**JCB4**	**JCB4**	**JCB4**	**JCBG**	**JCBG**	**JCBG**	**JCBG**	**JCBG**	**JCBG**
Spinel	0.05	0.06	0.12	0.01	0.00	0.08	0.13	0.05	0.11	0.23	0.04	0.00	0.21	0.00	0.00	0.00	0.00	0.00	0.00	0.00
Mg.Ulv.Spi	0.09	0.12	0.00	0.07	0.17	1.65	2.33	2.39	1.97	0.05	0.05	0.17	0.09	0.08	0.25	0.17	0.09	0.07	0.16	0.13
Mn.Ulv.Spi	0.18	0.35	0.59	0.55	0.13	1.39	0.76	0.83	0.95	0.25	0.14	0.15	0.18	0.23	0.15	0.27	0.13	0.03	0.18	0.00
Ulvospinel	0.00	0.00	0.21	0.06	0.00	0.00	0.00	0.00	0.00	0.00	0.17	0.00	0.35	0.07	0.00	0.12	0.00	0.18	0.26	0.00
Mn.Chromite	0.56	0.37	0.00	0.00	0.53	2.50	3.31	3.30	2.95	0.51	0.00	0.07	0.00	0.00	0.45	0.00	0.11	0.00	0.00	0.58
Mg.Chromite	0.00	0.00	0.00	0.00	0.00	0.00	0.00	0.00	0.00	0.00	0.00	0.00	0.00	0.00	0.00	0.00	0.00	0.00	0.00	0.11
Chromite	**4.78**	**6.06**	**5.83**	**3.93**	**4.26**	**12.91**	**12.49**	**12.93**	**13.43**	**6.56**	**6.84**	**6.41**	**7.58**	**6.94**	**2.47**	**3.35**	**3.03**	**2.73**	**3.10**	**2.76**
Magnetite	**94.34**	**93.05**	**93.26**	**95.37**	**94.92**	**81.48**	**80.98**	**80.50**	**80.59**	**92.40**	**92.76**	**93.21**	**91.59**	**92.69**	**96.69**	**96.08**	**96.63**	**96.99**	**96.30**	**96.43**
Total	100	100	100	100	100	100	100	100	100	100	100	100	100	100	100	100	100	100	100	100

Table 3. Cation proportions (apfu) of Magnetites.

Cation (apfu)	Magnetite																								
Sample No.	**JCB4**	**JCB4**	**JCB5**	**JCB5**	**JCB5**	**JCB5**	**JCB5**	**JCB5**	**JCB5**	**JCB5**	**JCB5**	**JCB5**	**JCB5**	**JCB5**	**JCB5**	**JCB5**	**JCB5**	**JCB5**	**JCB5**	**JCB5**	**JCB5**	**JCB5**	**JCB5**	**JCB5**	**JCB5**
Si	0.31	0.27	0.02	0.12	0.13	0.16	0.16	0.14	0.15	0.14	0.14	0.12	0.14	0.15	0.14	0.14	0.12	0.13	0.16	0.17	0.17	0.17	0.14	0.18	0.17
Ti	0.00	0.00	0.00	0.00	0.00	0.00	0.00	0.00	0.00	0.00	0.00	0.00	0.00	0.00	0.00	0.00	0.00	0.00	0.00	0.00	0.00	0.00	0.00	0.00	0.00
Al	0.06	0.05	0.02	0.00	0.00	0.00	0.00	0.00	0.00	0.00	0.00	0.00	0.00	0.00	0.00	0.00	0.00	0.00	0.00	0.00	0.00	0.00	0.00	0.00	0.00
Cr	0.01	0.00	0.00	0.00	0.00	0.00	0.00	0.00	0.00	0.00	0.00	0.00	0.00	0.00	0.00	0.00	0.00	0.00	0.00	0.00	0.00	0.00	0.00	0.00	0.00
Fe^{3+}	1.38	1.44	1.93	1.78	1.75	1.72	1.72	1.72	1.69	1.72	1.72	1.76	1.73	1.71	1.72	1.73	1.76	1.73	1.67	1.65	1.67	1.66	1.71	1.65	1.67
Fe^{2+}	1.09	0.92	1.00	1.02	1.10	1.07	1.06	1.12	1.13	1.13	1.12	1.09	1.11	1.13	1.13	1.12	1.09	1.11	1.14	1.16	1.15	1.15	1.11	1.17	1.15
Mn	0.01	0.00	0.00	0.00	0.00	0.00	0.00	0.00	0.00	0.00	0.00	0.00	0.00	0.00	0.00	0.00	0.00	0.00	0.00	0.00	0.00	0.01	0.00	0.00	0.00
Mg	0.02	0.03	0.00	0.00	0.00	0.01	0.01	0.00	0.00	0.00	0.00	0.00	0.00	0.00	0.00	0.00	0.00	0.00	0.00	0.00	0.00	0.00	0.01	0.00	0.00
Ca	0.02	0.20	0.00	0.01	0.01	0.01	0.01	0.01	0.01	0.00	0.01	0.01	0.01	0.00	0.00	0.01	0.01	0.01	0.00	0.00	0.01	0.00	0.00	0.00	0.00
Na	0.05	0.03	0.00	0.03	0.01	0.03	0.04	0.00	0.00	0.00	0.00	0.00	0.00	0.00	0.00	0.00	0.01	0.00	0.00	0.00	0.00	0.00	0.00	0.00	0.00
K	0.02	0.01	0.00	0.00	0.00	0.00	0.00	0.00	0.00	0.00	0.00	0.00	0.00	0.00	0.00	0.00	0.00	0.00	0.00	0.00	0.00	0.00	0.00	0.00	0.00
Ni	0.03	0.05	0.01	0.02	0.00	0.00	0.00	0.00	0.01	0.00	0.00	0.01	0.01	0.00	0.01	0.01	0.00	0.01	0.01	0.00	0.01	0.01	0.01	0.01	0.01
Total	**3.00**	**3.00**	**3.00**	**3.00**	**3.00**	**3.00**	**3.00**	**3.00**	**3.00**	**3.00**	**3.00**	**3.00**	**3.00**	**3.00**	**3.00**	**3.00**	**3.00**	**3.00**	**3.00**	**3.00**	**3.00**	**3.00**	**3.00**	**3.00**	**3.00**
Cr#	0.13	0.04	0.03	0.00	0.00	0.00	0.00	0.00	0.00	0.00	0.00	0.00	0.00	0.00	0.00	0.00	0.00	0.00	0.00	0.00	0.00	0.00	0.00	0.00	0.00
Mg#	0.02	0.03	0.00	0.00	0.00	0.01	0.01	0.00	0.00	0.00	0.00	0.00	0.00	0.00	0.00	0.00	0.00	0.00	0.00	0.00	0.00	0.00	0.01	0.00	0.00
Fe#	0.98	0.97	1.00	1.00	1.00	0.99	0.99	1.00	1.00	1.00	1.00	1.00	1.00	1.00	1.00	1.00	1.00	1.00	1.00	1.00	1.00	1.00	0.99	1.00	1.00
Fe^{3+}/R^{3+}	0.95	0.96	0.99	1.00	1.00	1.00	1.00	1.00	1.00	1.00	1.00	1.00	1.00	1.00	1.00	1.00	1.00	1.00	1.00	1.00	1.00	1.00	1.00	1.00	1.00
End Members																									
Sample No.	**JCB4**	**JCB4**	**JCB5**	**JCB5**	**JCB5**	**JCB5**	**JCB5**	**JCB5**	**JCB5**	**JCB5**	**JCB5**	**JCB5**	**JCB5**	**JCB5**	**JCB5**	**JCB5**	**JCB5**	**JCB5**	**JCB5**	**JCB5**	**JCB5**	**JCB5**	**JCB5**	**JCB5**	**JCB5**
Spinel	1.88	2.13	0.15	0.02	0.00	0.01	0.01	0.01	0.00	0.00	0.02	0.00	0.00	0.00	0.00	0.03	0.00	0.00	0.01	0.00	0.00	0.02	0.00	0.00	0.01
Mg.Ulv.Spi	0.00	0.00	0.00	0.00	0.02	0.07	0.00	0.05	0.01	0.00	0.00	0.13	0.01	0.00	0.02	0.00	0.00	0.05	0.00	0.00	0.04	0.01	0.05	0.00	0.03
Mn.Ulv.Spi	0.00	0.00	0.09	0.00	0.04	0.00	0.00	0.00	0.05	0.01	0.00	0.00	0.00	0.00	0.00	0.00	0.00	0.00	0.00	0.00	0.00	0.00	0.00	0.00	0.00
Ulvospinel	0.00	0.00	0.00	0.00	0.00	0.00	0.00	0.00	0.00	0.00	0.00	0.00	0.00	0.00	0.00	0.00	0.00	0.00	0.00	0.00	0.00	0.00	0.00	0.04	0.00
Mn.Chromite	0.37	0.03	0.02	0.00	0.00	0.00	0.00	0.00	0.00	0.02	0.00	0.00	0.05	0.00	0.00	0.00	0.00	0.01	0.01	0.00	0.00	0.00	0.00	0.00	0.00
Mg.Chromite	0.00	0.06	0.00	0.00	0.00	0.00	0.04	0.00	0.00	0.00	0.00	0.00	0.00	0.00	0.00	0.00	0.00	0.04	0.00	0.00	0.01	0.00	0.00	0.00	0.00
Chromite	0.00	0.00	0.00	0.00	0.00	0.00	0.00	0.00	0.00	0.00	0.00	0.00	0.00	0.00	0.00	0.00	0.00	0.00	0.00	0.00	0.00	0.00	0.00	0.00	0.00
Magnetite	**97.75**	**97.78**	**99.73**	**99.98**	**99.93**	**99.92**	**99.95**	**99.94**	**99.94**	**99.97**	**99.98**	**99.87**	**99.94**	**100.00**	**99.98**	**99.97**	**100.00**	**99.89**	**99.98**	**100.00**	**99.95**	**99.98**	**99.95**	**99.96**	**99.96**
Total	100	100	100	100	100	100	100	100	100	100	100	100	100	100	100	100	100	100	100	100	100	100	100	100	100

5. Discussion

Metallic deposits in layered sequences such as primary fractionated layers and late hydrothermal emplacements, are ubiquitous worldwide. The lithotypes present in the study area are layered sequences of ultramafic rocks (dunite-peridotite-pyroxenite) with magnetite mineralization as bands and veins. These rocks are affected by significant hydrothermal activity due to the metamorphic process and are entirely serpentinized, forming serpentinite with few residues of olivine and pyrox-

ene. The vein form of magnetite is formed during serpentinization and occurs on a centimetric scale, which is rarely observed in serpentinites [23].

A petrographic study of samples from layered ultramafic sequence rocks suggests that the ore and silicate minerals developed rhythmically and contemporaneously, primarily due to episodic injection of primitive magma, which cooled with moderate fractional crystallization and could have some genetic relationship with the main komatiitic suites. The layered sill could be a basal adcumulate part of komatiitic magma [8]. The mineral assemblage of serpentine + talc + chlorite + magnesite + tremolite indicates transition facies of greenschist to amphibolite facies metamorphism [8] [24]. The Reflected light microscope study of the samples reveals that the source rocks host oxide and sulfide ore mineral phases. EPMA data reveals that the opaques in layered sill are Cr-magnetite and magnetite (**Table 2** & **Table 3**).

Chrome spinel is a ubiquitous mineral in ultramafic rocks. Cr-magnetite and magnetite are the bimodal alteration phases developed in the spinel transformation system (Cr-Fe^{3+}) during the metamorphism or hydrothermal alteration exhibiting wide geochemical variation due to the varied substitutions of Fe and Cr. These spinel alteration phases are metamorphic grade indicators [23]-[25]. The formula for Cr-Fe^{3+} spinel series is

$$Fe^{2+}\left(Fe^{3+}_{1-n}Cr_n\right)_2 O_4$$

where $0 < n < 1$. The two end members of the system are pure chromite ($FeCr_2O_4$) for $n = 1$ and magnetite ($Fe^{2+}Fe^{3+}{}_2O_4$) for n = 0 [26] [27].

The alteration of chromite to Cr-magnetite to magnetite is marked by a decrease in Cr^{3+} and an increase in Fe^{3+}. Varying Cr^{3+} proportions are noticed in Cr-magnetite grains of the layered band (Cr3+: 0.023 - 0.2108 apfu) and vein forms (Cr^{3+}: 0.4266 - 0.4506 apfu), indicating multistage alteration. The Cr-magnetite grains are compositionally homogenous in veins with high Cr concentration values and have slight substitutions of Ti, Mn, Mg, and Al, which are two to three times higher than those in the layered bands. The atomic ratios in Cr-magnetite exhibit high Cr#[Cr/(Cr+Al)]: 0.95 - 1 atomic ratios; low Mg#[Mg/(Mg + Fe^{2+})]: 0.0013 - 0.0470 atomic ratios, and depleted Al of 0.0015 apfu, which shows substantial alteration of the primary chromite [28]-[30]. Cr shows a positive correlation with Mg, Mn, and Ti, no correlation with Al and Ni, and a negative correlation with Fe^{3+}, Fe^{2+}, and Fe^{3+}/R^{3+} where R^{3+} is Cr+Al+Fe^{3+} (**Figure 8**). The high Fe^{3+}: 1.376 - 1.933 apfu; high Fe^{2+}#[Fe^{2+}/(Fe^{2+}+Mg)]: 0.97 - 1.00 atomic ratios; and depleted Cr^{3+}: 0 - 0.0094 apfu; Mg: 0 - 0.034 apfu; Al: 0 - 0.0011 apfu, indicates the complete transformation of spinel to Magnetite. The Cr-spinels are prone to solid alterations during prograde to retrograde metamorphism of host rocks and hydrothermal alteration [24] [31]. The chromite grains are wholly transformed into Cr-magnetite at amphibolite facies metamorphism with enriched Fe^{3+} and later into magnetite at greenschist facies metamorphism due to the reducing conditions [8] [24]. The altered opaque grains are depleted with Cr, Mg, Al, and Ni due to

their redistribution under extreme stages of metamorphism. The EPMA data of studied oxide phases plotting midway of the Cr-Fe^{3+} line in trivalent ions (Cr-Al-Fe^{3+}) ternary plot and falls within the fields of metamorphogenic magnetite of greenschist to amphibolite facies [31] (**Figure 9**). The plot of Mg# vs. Fe^{3+}/R^{3+} (R^{3+} = Cr + Al + Fe^{3+}) and Fe# vs. Fe^{3+}/R^{3+} reveals highly altered compositions characterized by strong enrichment of Fe^{3+} in metamorphogenic magnetite (**Figure 10**). All Cr-magnetite samples except a few plots in between Cr-magnetite and magnetite represent additional miscibility gaps in bimodal phases of the Cr-Fe^{3+} transformation series of the Cr-Al-Fe^{3+} ternary plot [31], and these varieties are termed as ishkulite [32] [33], as the Cr^{3+} proportions range between 0.10 to 0.4506 apfu of studied samples matches with the 0.10 - 0.50 apfu of ishkulite in open database of minerals in mindat.org [34] (**Figure 9**). Compositional variation is expected in chromites in ultramafic rock due to subsolidus re-equilibration of the chromites with surrounding silicates and interstitial melt [5] [8] [35]-[39]. The chromite grains alter due to hydrothermal effects (serpentinization) and metamorphism by reducing and then oxidizing by highly oxidizing fluid. During this process, chromite grains completely alter to homogenous Cr-magnetite [8]. During the hydrothermal alteration the interaction of thermal fluids with iron bearing minerals (olivine, pyroxenes and accessory chromites) in ultramafic rocks could cause the release of the reducing agents and lead to the formation of Cr-magnetite with an increase in Fe^{3+} by diffusion through oxidizing fluids. Metamorphic process facilitates the oxidation transformation of chromite grains as the temperature and pressure increase, causing breakdown by releasing chromium and iron and then recombine to form bimodal phases of ferrit-chromite and Cr-magnetite in spinel transformation system. This process involves primarily the oxidation of chromium and reduction of iron. Chromite ($Fe^{2+}Cr_2O_4$) containing chromium in +3 oxidation state is oxidized to +6 state forming soluble chromate ions. Simultaneously, iron in chromite in +2 is reduced to a +3 state, to form as magnetite ($Fe^{2+}Fe_2^{3+}O_4$).

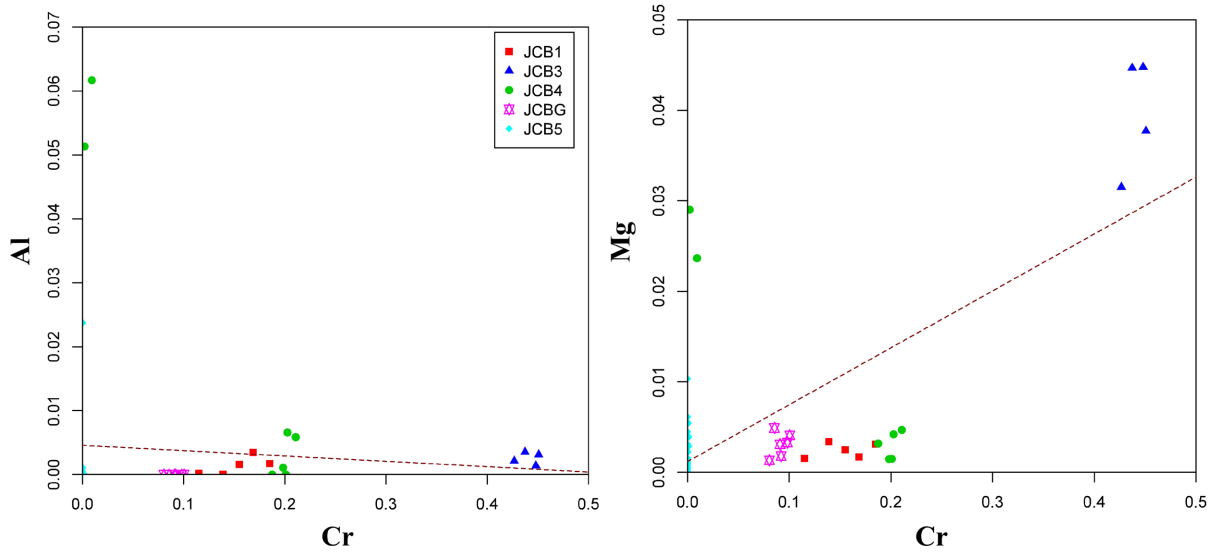

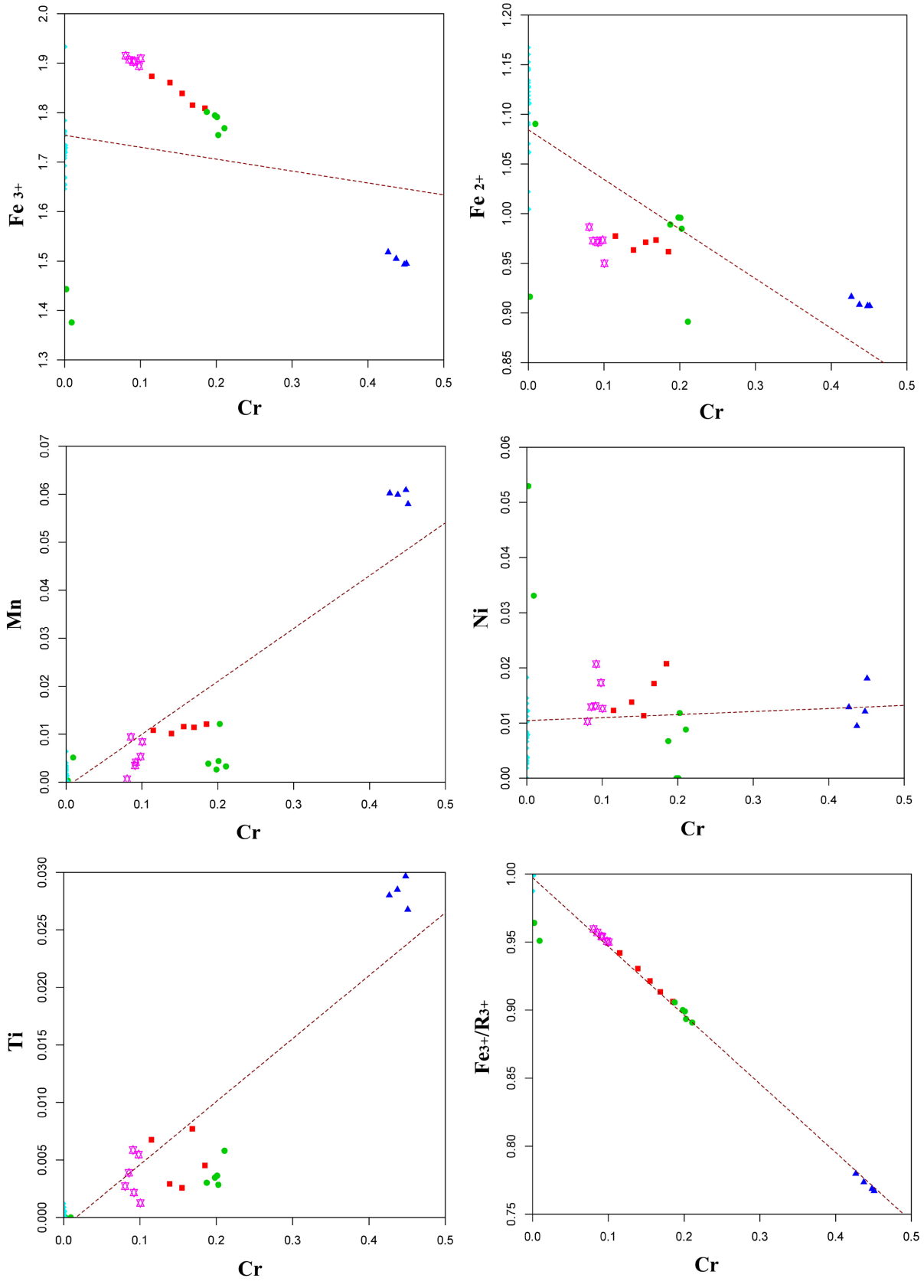

Figure 8. Scatter plot for correlation of Cr with other major and minor elements.

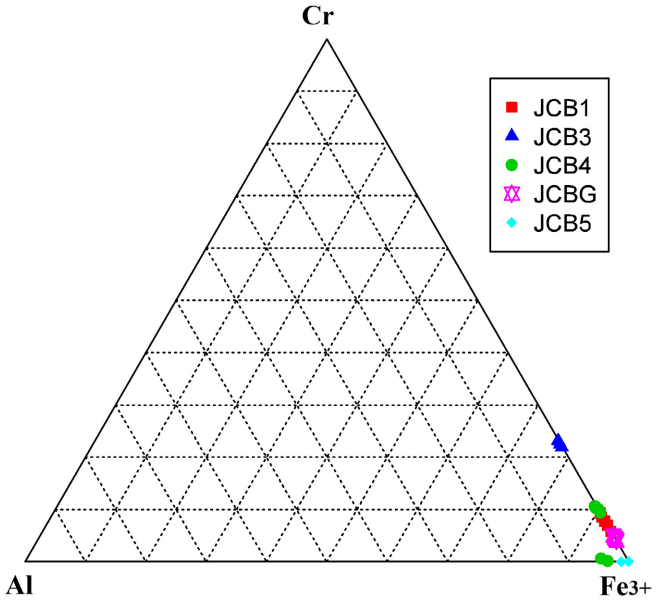

Figure 9. Ternary plot of trivalent ions Cr-Al-Fe^{3+} (Barnes, 2001).

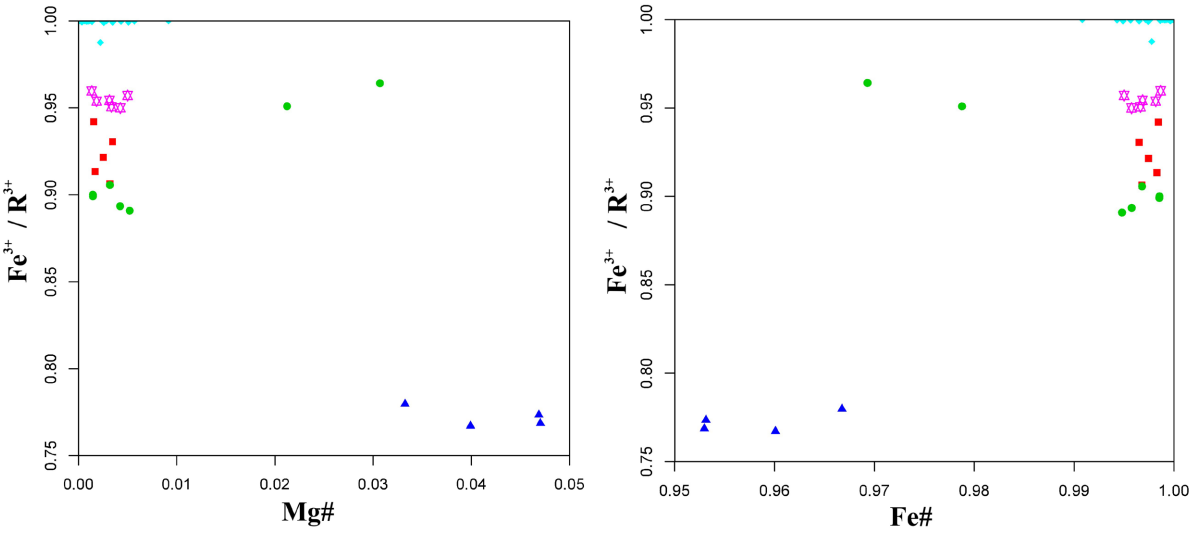

Figure 10. Binary plot of Mg# vs. Fe^{3+}/R^{3+} and Fe# vs. Fe^{3+}/R^{3+}.

6. Conclusion

In the outcrops, mineralization is observed as bands in adcumulate ultramafic rocks of the layered sill and as veins in adjacent serpentinites. Petrographic and EPMA studies of opaques reveal Cr-magnetite and magnetite. The terrain has suffered an episodic prograde to retrograde metamorphism of greenschist to amphibolite facies with significant alteration of precursor rocks and minerals. Precursor chromite grains are completely transformed into homogenous Cr-magnetite and magnetite due to hydrothermal alteration and metamorphic process. During the transformation process, the elements Cr, Mg, Al, Mn, and Ni are depleted, and Fe3+ is enriched significantly. Cr-magnetite, representing an additional miscibility

gap, is of the Ishkulite variety. Cr-magnetite appearing as centimeter-scale veins is mainly due to serpentinization, and such occurrences are rare in serpentinite. The cation concentrations of Cr-magnetite in vein form with significant Cr concentration and slight substitutions of Ti, Mg, Mn, and Al show the opposite trend with respect to the other metamorphogenic magnetites, indicating later hydrothermal alteration in episodic metamorphism. The layered sill appears to be the lower adcumulate part of the komatiite suite. The presence of Cr-magnetite as the vein in the study area would indicate possible chromite deposits hidden beneath, and the magnetite grains subjected to hydrothermal alterations could host noble metals like gold and PGEs. The present findings are new and are the result of a preliminary investigation. Hence, there is a scope for detailed studies to understand the full potential of mineralization.

Acknowledgements

We thank Prof. N. V. Chalapathi Rao, presently Director, National Centre for Earth Science Studies (MoES), Thiruvananthapuram, and earlier Professor, Department of Geology, Centre of Advanced Study, Institute of Science, Banaras Hindu University, India, for granting permission and extending support to conduct EPMA studies at their Laboratory. We also thank Dr. Rohit Pandey, Assistant Professor, Mantle Petrology Lab, Department of Geology, Centre of Advanced Study, Institute of Science, Banaras Hindu University, India, for extending kind support in EPMA analysis. Prof. N. Malarkodi, the Chairperson, Department of Geology, Bangalore University, India, and Prof. P. C. Nagesh, Former Chairperson, Department of Geology, Bangalore University, India, are thankful for their support during the course of our work.

Conflicts of Interest

The authors declare no conflicts of interest regarding the publication of this paper.

References

[1] Latypov, R.M., Namur, O., Bai, Y., Barnes, S.J., Chistyakova, S., Holness, M.B., *et al.* (2024) Layered Intrusions: Fundamentals, Novel Observations and Concepts, and Controversial Issues. *Earth-Science Reviews*, **249**, Article 104653. https://doi.org/10.1016/j.earscirev.2023.104653

[2] Arndt, N.T. (1986) Differentiation of Komatiite Flows. *Journal of Petrology*, **27**, 279-301. https://doi.org/10.1093/petrology/27.2.279

[3] Lahaye, Y., Arndt, N., Byerly, G., Chauvel, C., Fourcade, S. and Gruau, G. (1995) The Influence of Alteration on the Trace-Element and Nd Isotopic Compositions of Komatiites. *Chemical Geology*, **126**, 43-64. https://doi.org/10.1016/0009-2541(95)00102-1

[4] Jayananda, M., Kano, T., Peucat, J. and Channabasappa, S. (2008) 3.35Ga Komatiite Volcanism in the Western Dharwar Craton, Southern India: Constraints from Nd Isotopes and Whole-Rock Geochemistry. *Precambrian Research*, **162**, 160-179. https://doi.org/10.1016/j.precamres.2007.07.010

[5] Mukherjee, R., Mondal, S.K., Rosing, M.T. and Frei, R. (2010) Compositional Variations in the Mesoarchean Chromites of the Nuggihalli Schist Belt, Western Dharwar Craton (India): Potential Parental Melts and Implications for Tectonic Setting. *Contributions to Mineralogy and Petrology*, **160**, 865-885. https://doi.org/10.1007/s00410-010-0511-5

[6] Prabhakar, B.C. and Namratha, R. (2014) Morphology and Textures of Komatiite Flows of J.C. Pura Schist Belt, Dharwar Craton. *Journal of the Geological Society of India*, **83**, 13-20. https://doi.org/10.1007/s12594-014-0002-9

[7] Sappin, A.-A., Houlé, M.G., Lesher, C.M., McNicoll, V., Vaillancourt, C. and Kamber, B.S. (2016) Age Constraints and Geochemical Evolution of the Neoarchean Mafic-Ultramafic Wabassi Intrusive Complex in the Miminiska-Fort Hope Greenstone Belt, Superior Province, Canada. *Precambrian Research*, **286**, 101-125. https://doi.org/10.1016/j.precamres.2016.09.018

[8] Banerjee, R., Biswas, B.K. and Mondal, S.K. (2023) Origin of Alteration Patterns in Accessory Chromites from the Kudada Metaperidotites, East Singhbhum District (Jharkhand, India). *Journal of the Geological Society of India*, **99**, 345-356. https://doi.org/10.1007/s12594-023-2317-x

[9] Venkata Dasu, S.P., Ramakrishnan, T.M. and Mahabaleswar, B. (1991) Sargur-dharwar Relationship around the Komatiite-Rich Jayachamarajapura Greenstone Belt in Karnataka. *Journal Geological Society of India*, **38**, 577-592. https://doi.org/10.17491/jgsi/1991/380604

[10] Prabhakar, B.C. and Namratha, R. (2015) A Note on the Layered Dunite-Peridotite-Pyroxenite Sill in the Komatiitic Milieu of J.C. Pura Belt, Dharwar Craton. *Journal of Geological Society of India*, **85**, 120-121.

[11] Santhosh, S., Dayanand, B.G. and Prabhakar, B.C. (2023) Geochemistry of Layered Ultramafic Rocks in J.C. Pura Schist Belt, Dharwar Craton, Karnataka, India. *Open Journal of Geology*, **13**, 189-202. https://doi.org/10.4236/ojg.2023.132009

[12] Rashmi, B. N., Prabhakar, B. C., Gireesh, R. V., Nijagunaiah, R., and Ranganath, R. M. (2009) Nickel Anomalies in Ultramafic Profiles of Jayachamarajapura Schist Belt, Western Dharwar Craton. *Current Science*, 96, 1512-11517. http://www.jstor.org/stable/24104781

[13] Fayazudeen, P.J., Sahoo, H.B., Das, P., Datta, D. and Taye, S.K. (2019) Reconnaissance Survey for Ni-PGE and Gold between Rampura and Gollarahatti Areas of J.C. Pura Mafic-Ultramafic Belt, Hassan District, Karnataka (Stage-G4). Technical Report, Geological Survey of India.

[14] Talukdar, D., Singh, A., Raul, A.K., Mandal, N., Mohanty, S.N., Mohanty, M. and Korakoppa, M.M. (2018) Occurrence of Precious Metals in Ultramafic Hosted Magnetite of J. C. Pura Belt, Western Dharwar Craton, Karnataka. *Indian Journal of Geoscience*, **72**, 175-184.

[15] Ramakrishnan, M., Venkata Dasu, S.P. and Kroener, A. (1994) Middle Archaean Age of Sargur Group by Single Grain Zircon Dating and Geochemical Evidence for the Clastic Origin of Metaquartzite from J. C. Pura Greenstone Belt, Karnataka. *Journal Geological Society of India*, **44**, 605-616. https://doi.org/10.17491/jgsi/1994/440602

[16] Naqvi, S.A., Govil, P.K. and Rogers, J.J.W. (1981) Chemical Sedimentation in Archaean-Early Proterozoic Greenstone Belts of the Dharwar Craton, India. In: Glover, J.E. and Groves, D.I., Eds., *Archean Geology*: *Second International Symposium*, *Perth*, No. 7, Geological Society of Australia, 245-254.

[17] Chardon, D., Choukroune, P., Jayananda, M. (1996) Strain Patterns, Décollement and Incipient Sagducted Greenstone Terrains in the Archaean Dharwar Craton (South

India). *Journal of Structural Geology*, **18**, 991-999, 1001-1004. https://doi.org/10.1016/0191-8141(96)00031-4

[18] Philpotts, A. and Ague, J. (2009) Principles of Igneous and Metamorphic Petrology. 2nd Edtion, Cambridge University Press. https://doi.org/10.1017/cbo9780511813429

[19] Jayananda, M., Duraiswami, R.A., Aadhiseshan, K.R., Gireesh, R.V., Prabhakar, B.C., Kafo, K., *et al.* (2016) Physical Volcanology and Geochemistry of Palaeoarchaean Komatiite Lava Flows from the Western Dharwar Craton, Southern India: Implications for Archaean Mantle Evolution and Crustal Growth. *International Geology Review*, **58**, 1569-1595. https://doi.org/10.1080/00206814.2016.1172350

[20] Pandey, R., Rao, N.V.C., Pandit, D., Sahoo, S. and Dhote, P. (2017) Imprints of Modal Metasomatism in the Post-Deccan Subcontinental Lithospheric Mantle: Petrological Evidence from an Ultramafic Xenolith in an Eocene Lamprophyre, NW India. *Geological Society, London, Special Publications*, **463**, 117-136. https://doi.org/10.1144/sp463.6

[21] Hatert, F., Mills, S.J., Pasero, M. and Williams, P.A. (2013) CNMNC Guidelines for the Use of Suffixes and Prefixes in Mineral Nomenclature, and for the Preservation of Historical Names. *European Journal of Mineralogy*, **25**, 113-115. https://doi.org/10.1127/0935-1221/2013/0025-2267

[22] Bosi, F., Biagioni, C. and Pasero, M. (2019) Nomenclature and Classification of the Spinel Supergroup. *European Journal of Mineralogy*, **31**, 183-192. https://doi.org/10.1127/ejm/2019/0031-2788

[23] Florent, H., Mélina, M., Julie, C., Antoine, T., Julien, B., Ricardo, T., *et al.* (2017) Identification of Cr-Magnetite in Neoproterozoic Serpentinites Resulting of Cr-Spinel Alteration in a Past Hydrothermal System: Aït Ahmane ultramafic unit (Bou Azzer ophiolite, Anti Atlas, Morocco). 19*th EGU General Assembly*, *EGU*2017, *Proceedings from the Conference*, Vienna, 23-28 April 2017, 13876. https://ui.adsabs.harvard.edu/abs/2017EGUGA..1913876H/abstract

[24] Barnes, S.J. (2000) Chromite in Komatiites, II. Modification during Greenschist to Mid-Amphibolite Facies Metamorphism. *Journal of Petrology*, **41**, 387-409. https://doi.org/10.1093/petrology/41.3.387

[25] Ahmed, A.H. and Surour, A.A. (2016) Fluid-Related Modifications of Cr-Spinel and Olivine from Ophiolitic Peridotites by Contact Metamorphism of Granitic Intrusions in the Ablah Area, Saudi Arabia. *Journal of Asian Earth Sciences*, **122**, 58-79. https://doi.org/10.1016/j.jseaes.2016.03.010

[26] Hodel, F., Macouin, M., Trindade, R.I.F., Araujo, J.F.D.F., Respaud, M., Meunier, J.F., *et al.* (2020) Magnetic Properties of Ferritchromite and Cr-magnetite and Monitoring of Cr-Spinels Alteration in Ultramafic and Mafic Rocks. *Geochemistry, Geophysics, Geosystems*, **21**, GC009227. https://doi.org/10.1029/2020gc009227

[27] Ziemniak, S.E. and Castelli, R.A. (2003) Immiscibility in the Fe_3O_4-$FeCr_2O_4$ Spinel Binary. *Journal of Physics and Chemistry of Solids*, **64**, 2081-2091. https://doi.org/10.1016/s0022-3697(03)00237-3

[28] Diella, V., Ferrario, A. and Rossetti, P. (1994) The Magnetite Ore Deposits of the Southern Aosta Valley: Chromite Transformed during an Alpine Metamorphic Event. *Ofioliti*, **19**, 247-256.

[29] Rossetti, P., Gatta, G.D., Diella, V., Carbonin, S., Della Giusta, A. and Ferrario, A. (2009) The Magnetite Ore Districts of the Southern Aosta Valley (Western Alps, Italy): A Mineralogical Study of Metasomatized Chromite Ore. *Mineralogical Magazine*, **73**, 737-751. https://doi.org/10.1180/minmag.2009.073.5.737

[30] Giusta, A.D., Carbonin, S. and Umberto, R. (2011) Chromite to Magnetite Transfor-

mation: Compositional Variations and Cation Distributions (Southern Aosta Valley, Western Alps, Italy). *Periodico di Mineralogia*, **80**. 1-17. https://doi.org/10.2451/2011PM0001

[31] Barnes, S.J. and Roeder, P.L. (2001) The Range of Spinel Compositions in Terrestrial Mafic and Ultramafic Rocks. *Journal of Petrology*, **42**, 2279-2302. https://doi.org/10.1093/petrology/42.12.2279

[32] Sergeyeva, N.G. (1969) Ishulite under Electronic Microscope. *International Geology Review*, **11**, 401-405. https://doi.org/10.1080/00206816909475068

[33] Malitch, K.N. and Auge, T. (1998) The Composition of Inclusions in Osmium Minerals as an Indicator of the Formation Conditions of the Guli Ultramafic Massif. *Doklady Earth Sciences*, **361A**, 812-814.

[34] Ishkulite. https://www.mindat.org/min-9875.html

[35] Irvine, T.N. (1967) Chromian Spinel as a Petrogenetic Indicator: Part 2. Petrologic Applications. *Canadian Journal of Earth Sciences*, **4**, 71-103. https://doi.org/10.1139/e67-004

[36] Cameron, E.N. (1975) Postcumulus and Subsolidus Equilibration of Chomite and Coexisting Silicates in the Eastern Bushveld Complex. *Geochimica et Cosmochimica Acta*, **39**, 1021-1033. https://doi.org/10.1016/0016-7037(75)90044-7

[37] Roeder, P.L. and Campbell, I.H. (1985) The Effect of Postcumulus Reactions on Composition of Chrome-Spinels from the Jimberlana Intrusion. *Journal of Petrology*, **26**, 763-786. https://doi.org/10.1093/petrology/26.3.763

[38] Scowen, P.A.H., Roeder, P.L. and Helz, R.T. (1991) Reequilibration of Chromite within Kilauea Iki Lava Lake, Hawaii. *Contributions to Mineralogy and Petrology*, **107**, 8-20. https://doi.org/10.1007/bf00311181

[39] Rollinson, H. (1995) Composition and Tectonic Settings of Chromite Deposits through Time; Discussion. *Economic Geology*, **90**, 2091-2092. https://doi.org/10.2113/gsecongeo.90.7.2091